Simplify your imaging workflows

Make research imaging workflows accessible, traceable, and secure with Athena Software for Core Imaging Facilities.

Thermo Scientific™ Athena Software is a premium imaging data management platform designed for core imaging facilities that support materials science research.

Athena Software ensures traceability of images, metadata, and experimental workflows through an intuitive and collaborative web interface.

Find out more at **thermofisher.com/athena**

ThermoFisher SCIENTIFIC

ADVANCED OPTICAL MATERIALS
www.advopticalmat.de

Mechanical and Self-Deformable Spatial Modulation Beam Steering and Splitting Metasurface

*Ratanak Phon, Yeonju Kim, Eiyong Park, Heijun Jeong, and Sungjoon Lim**

Metasurfaces or artificial electromagnetic structures, offer feasible options to manipulate electromagnetic waves with compact and planar form factors. Tuneable metasurfaces can steer and split the electromagnetic wavefront, and are strongly desirable for many engineering and science applications. However, realizing tuneable metasurfaces that can achieve integrated diversified functionalities is somewhat challenging. This work proposes a simple spatial modulation mechanism to realize beam steering and splitting between left-handed and right-handed circularly polarized waves. A prototype proposed structure using 4D printing is fabricated to provide mechanical and self-deformation flexibility with different operating modes. Underlying concepts are confirmed and verified by theoretical predictions, numerical simulations, and experiments.

1. Introduction

Controlling light or electromagnetic wavefront propagation has been of great interest and importance for science and engineering research. Classical approaches use optical path elements and specific prism and lens shapes to accumulate phase changes. Metamaterials and metasurfaces (2D planar metamaterials) have attracted significant attention during the last two decades due to their ability to control electromagnetic fields in ways not found in natural materials.[1–3] Electromagnetic functionality can be achieved by controlling electromagnetic parameters such as permittivity (ε) and permeability (μ), in particular, controlling subwavelength array antennae orientation imprinting on the structures. Thus, metamaterials and metasurfaces are suitable for many applications from microwave to visible domains, including perfect lensing or superlenses,[4–6] invisibility cloaking,[7–9] beam deflectors,[10–12] holograms,[13,14] information processing, and analogue computation.[15–17]

R. Phon, Y. Kim, E. Park, H. Jeong, Prof. S. Lim
School of Electrical and Electronics Engineering
Chung-Ang University
Heukseok-Dong, Dongjak-Gu, Seoul 06974, Republic of Korea
E-mail: sungjoon@cau.ac.kr

The ORCID identification number(s) for the author(s) of this article can be found under https://doi.org/10.1002/adom.202100821.

DOI: 10.1002/adom.202100821

Dynamic beam-steering electromagnetic waves are traditionally achieved using phased array antennae, where individual phase shifter modules independently control phase profiles for each antenna element.[18–20] However, these are bulky, expensive, and require high complexity hardware such as digital-to-analogue (DACs) and analogue-to-digital (ADCs) converters, mixers, and power amplifiers. Discrete phase shifting, also called phase discontinuity, at metasurface interfaces offers a feasible method to shape or redirect the incidence electromagnetic wavefront.[21] This functionality is realized by designing different unit cell element phase profiles in the metasurfaces. The concept was implemented into digital coding metasurfaces that bridge between the digital and physical world and allow metamaterials/metasurfaces to process digital information directly, that is, information metamaterials.[22–25]

Polarization control, for example, splitting circularly polarized electromagnetic waves, with additional beam steering functionality is desirable for various applications from microwave to terahertz regimes. Most metasurface designs achieve abrupt phase changes by controlling unit cell structural dimensions to shift the resonance frequency and hence, alter the phase. Geometric phase metasurfaces, also known as Pancharatnam–Berry (PB) metasurfaces, can establish anisotropic phase gradient conveniently for manipulating circularly polarized (CP) waves.[26,27] Desirable phase-gradients can be achieved by controlling the local orientation for each unit cell, which is hardly to implement or integrate with active components such as varactors, PIN diodes, transistors, or other active materials to realize dynamically controllable PB metasurfaces. Most previous PB metasurfaces were passive structures with fixed functionality,[28–33] and it remains challenging to simultaneously realize beam steering and splitting between left-hand circularly polarized (LHCP) and right-hand circularly polarized (RHCP) waves in a single structure design, as discussed above.

In this work, we present a simple spatial modulation mechanism to simultaneously achieve beam steering and splitting functionality for LHCP and RHCP waves. The proposed structure is designed by combining the geometric phase concept and kirigami transformation mechanism, as illustrated in **Figure 1**. We extend the designed structure using 4D printing technology, providing a feasible way to achieve mechanical deformation (shape programming) and self-recovery

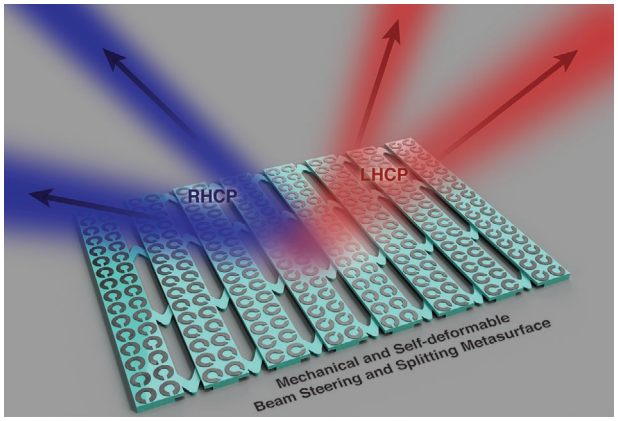

Figure 1. Conceptual illustration of the proposed mechanical and self-deformable spatial modulation metasurface. The metasurface is formed from smart material shape-memory polymer (SMP) that can mechanically deform and self-recover back to its original state. A single metasurface can be used to simultaneously realize beam splitting functionality between left-handed circularly polarized (LHCP) and right-handed circularly polarized (RHCP) waves and beam steering capability.

functionality. The transformability of the metasurface allows the beam-steering capability for the electromagnetic waves by mechanically deforming or self-recovering the shape of the proposed metasurface, which is demonstrated with the experiment results. The theoretical analysis and numerical simulation using the finite element method are used to study and predict spatial modulation mechanism behavior and the relation between geometric parameters of the metasurfaces and the metasurface performances. Experimental results confirm good agreement with analytical calculations and numerical simulations.

2. Results and Discussion

2.1. Circular–Polarization Beam Steering and Splitting Metasurface

Figure 2a shows the schematic illustration of the proposed circular polarized beam splitting and steering metasurface, in which designs with the orientation angle-dependent follow the notion of the geometric phase structure. It is worth mentioning that the arrangement of the phase distribution following this concept will allow obtaining the beam splitting functionality between LHCP and RHCP waves under a linear polarized incident electromagnetic wave. The proposed metasurface consists of eight metastrip elements, which can be transformed along the *x*-direction. The deformation along this *x*-axis will allow achieving beam steering functionality in the *xz* plane that will be demonstrated numerically and experimentally in the following section. Figure 2b shows the unit cell geometry of the proposed structure, which consists of a split-ring resonator (SRR) on the top and ground on the bottom layers. The optimized physical dimensions of the proposed structure are as follows: $p = 7.5$ mm, $c = 0.8$ mm, $\Lambda = 15$ mm, $R = 3.4$ mm, and $r = 1.8$ mm. In this work, we used a high temperature (HT) filament (dielectric constant $\varepsilon_r = 2$, loss tangent $\delta = 0.02$) as the intermediate dielectric substrate with a thickness $t = 2.6$ mm, whereas conductive patterns were made by silver coating with the conductivity of 61 000 000 S m^{-1}.

To examine and expect the electromagnetic functionality of the proposed metasurface, we first analyze the unit cell to find out its electromagnetic responses. We assume that the incoming electromagnetic wave illuminates the structure in the −*z*-direction. Figure 2c–e shows the simulated magnitudes and phases for four different orientation angles of the SRR

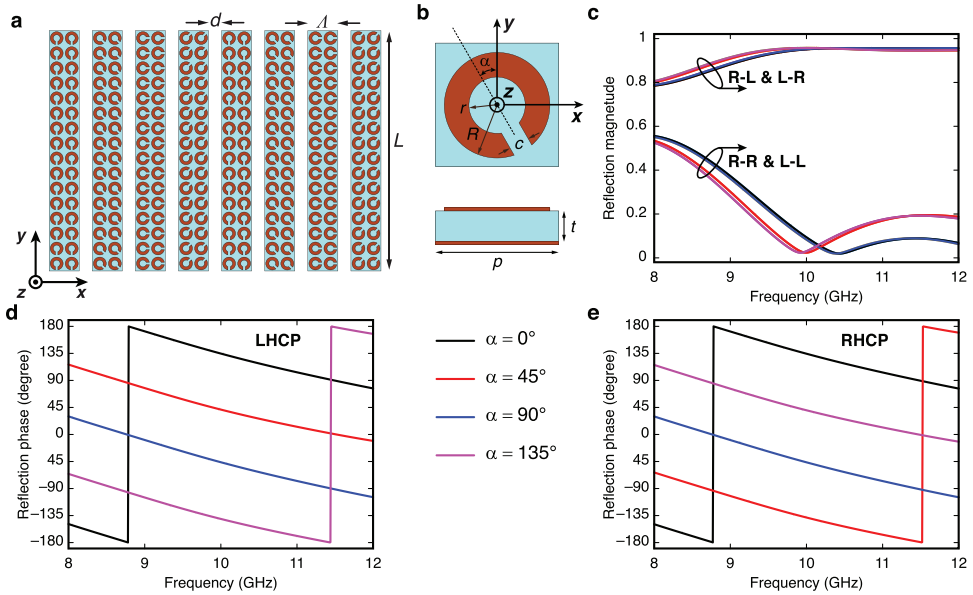

Figure 2. Circularly polarized beam steering and splitting metasurface. a,b) Proposed metasurface geometry comprising eight metastrips with split-ring resonator unit cells at four different orientation angles ($\alpha = 0°$, 45°, 90°, and 135°). c) Corresponding simulated reflected magnitude for co-polarization (R–R and L–L) and cross-polarization (R–L and L–R) channels. d,e) Simulated reflected phases for cross-polarization (R–L and L–R) channels where left-hand circularly polarized (LHCP) and right-hand circularly polarized (RHCP) output waves have opposite output phases.

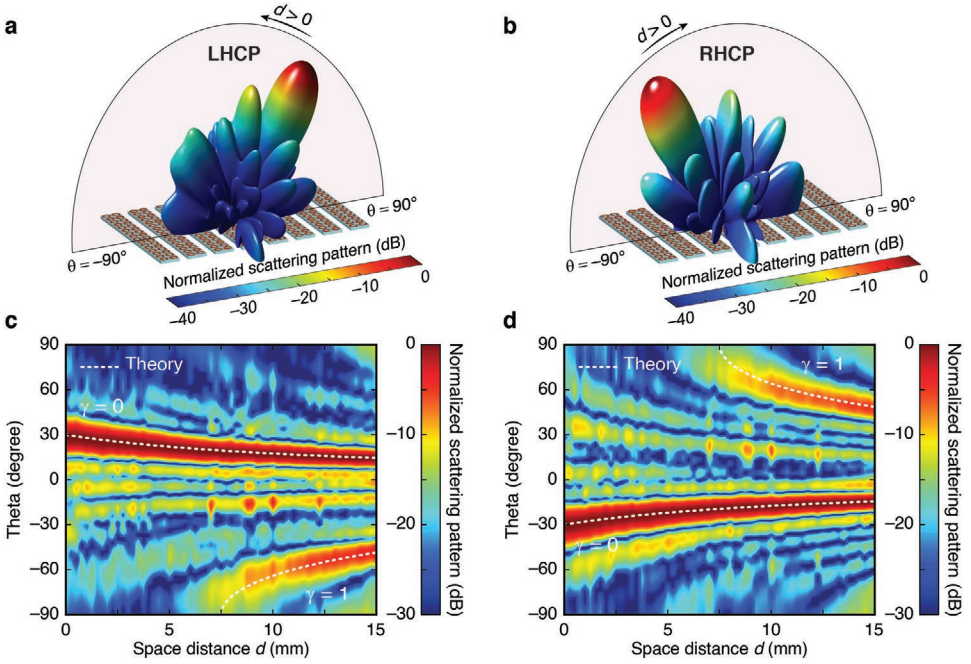

Figure 3. Electromagnetic functionality for the proposed circularly polarized beam steering and splitting metasurface. Simulated 3D normalized scattering patterns at 10 GHz and corresponding normalized 2D far-field scattering patterns for d = 0–15 mm for a,c) left-handed circularly polarized (LHCP), and b,d) right-handed circularly polarized (RHCP) output waves, respectively.

($\alpha = 0°$, 45°, 90°, and 135°) with respect to the y-axis. As shown in Figure 2c, we notice that the simulated magnitude for the cross-polarized channels (L–R, RHCP output under LHCP input, and R–L, LHCP output under RHCP input) are higher than two co-polarized channels (L–L, LHCP output under LHCP input, and R–R, RHCP output under RHCP input). These two-output cross-polarizations provide good phase variation over 360° phase shift for both L–R and R–L, as shown in Figure 2d,e. Phase differences for LHCP and RHCP output are $\Delta\psi_{R-L} \approx -90°$ and $\Delta\psi_{L-R} \approx +90°$, respectively. Now, we simulate the full metasurface (Figure 2a) in case of spatial distance d = 0 to find out its electromagnetic responses. We assume a linear polarized incident wave with an electric field along the y-axis illuminating the structure. **Figure 3**a,b shows the simulated results for 3D far-field radiation patterns for LHCP and RHCP waves. We observe that the deflection output waves at zeroth order mode (θ_0) can be split into LHCP and RHCP waves at +30° and −30°, respectively. Theoretical prediction for the LHCP and RHCP output beam can be expressed as

$$\theta_\gamma = \sin^{-1}\left[\pm\left(\frac{1}{4}-\gamma\right)\frac{\lambda}{\Lambda+d}\right] \quad (1)$$

respectively, where γ= 0, 1, 2, ... and θ_γ is the γorder deflection angle. The boundary condition for the deflection angle order from Equation (1) is

$$0 \le \gamma \le \frac{\Lambda+d}{\lambda}+\frac{1}{4} \quad (2)$$

To illustrate the beam steering capability of the spatial modulation mechanism, we perform a parametric study for the spatial distance d. As shown in Figure 3c,d, the LHCP and RHCP beams can be steered from ±30 to ±14°, respectively, as d increases from 0 to 15 mm. We notice that the first-order mode for LHCP and RHCP output waves can be obtained when d starts increasing from 7.5 mm. From the result in Figure 3c,d, we can observe a reasonable agreement between numerical simulation and theoretical prediction.

2.2. Fabrication and Experimental Verification

To experimentally validate the proposed design performance, the prototype of the circularly polarized beam steering and splitting metasurface in **Figure 4**a was fabricated using 4D printing technology and characterized in the microwave region. We used high temperature (HT) filaments as the supporting substrate with silver coating on the top and shape memory polymer (SMP) for mechanical deformation. Thus, the sample can deform shape (mechanical deformation or shape programming) and return to its original (self-deformation or shape recovery) with appropriate heating. Note S1, Supporting Information, provides detailed structure and geometry, and the fabrication process is detailed in the Experimental Section.

It should be noted that, consistent with previous works, reported metasurfaces were designed based on mechanical strain to switch the electromagnetic functionality.[34,35] For instance, they were designed and fabricated based on stretchable materials such as polydimethylsiloxane (PDMS) that is restricted to the stretching ratio. For metasurface, on the other hand, the conductive patterns imprinted on the stretchable materials can also deform their shape, while applying mechanical strains leading to unpredictable results with minor

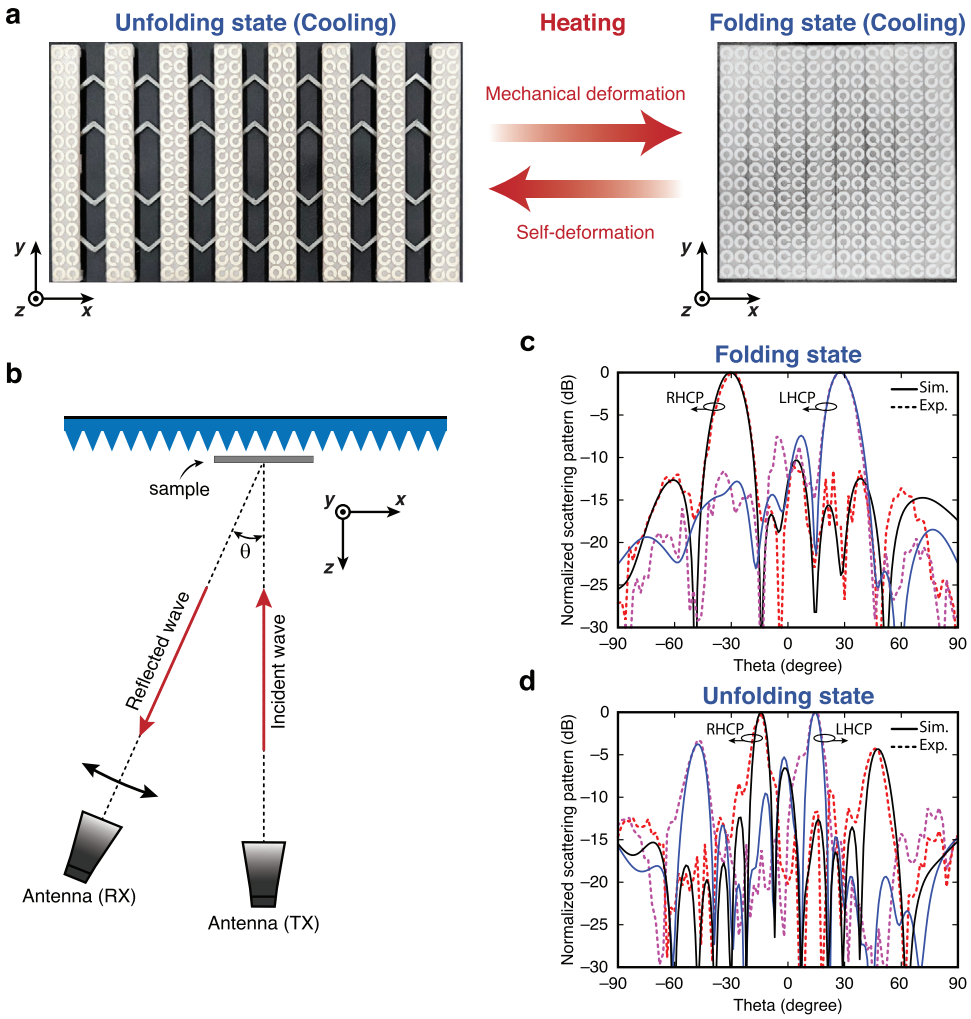

Figure 4. Fabricated prototype and experimental validation of the circularly polarized beam steering and splitting metasurface. a) Photograph of the fabricated prototype in unfolding ($d = 15$ mm) and folding ($d = 0$) states. b) Experimental configuration to measure reflection scattering pattern. c,d) Comparison between numerical simulation and measurement results for left-handed (LHCP) and right-handed circularly polarized (RHCP) output waves in c) folding and d) unfolding state.

performances. Especially, they required a mechanical system to hold the structure while applying the stains. In contrast, our proposed metasurface was designed based on a stretching kirigami mechanism (Figure S1, Supporting Information) that can provide a high deformation ratio (extension ratio) compared to stretchable materials like PDMS. The conductive pattern imprinted on the metastrip does not deform their shape while performing the mechanical deformation. This can minimize the parametric study condition in the design process. As we mentioned above, the proposed structure was designed using 4D printing technology, which can achieve mechanical deformation and self-recovery with appropriate heating. Therefore, it does not require a supporting mechanism to hold the structure like the stretchable material.

To experimentally validate the beam steering capability of the proposed structure, we consider two states as $d = 0$ and 15 mm in the experiment, which correspond to folded and unfolded states for the fabricated sample. Figure 4a shows the photograph of the fabricated sample in two different modes, which can deform from unfolding to folding states by applying heat and perform mechanical deformation using external force. The structure will remember its shape after cooling down to room temperature. In contrast, the deformation from folding to unfolding states can be achieved simply by applying heat, returning to the original shape due to SMP characteristics. For this experiment, we heated the fabricated sample to 60 °C to realize both working modes. Figure 4b shows the measurement setup to characterize the fabricated sample electromagnetic functionality (see Experimental Section for more details). An X-band lens horn antenna transmitted linear polarized plane waves on the sample at 10 GHz with electric fields along the *y*-axis. Electric field magnitudes and phases were measured at the receiver using a horn antenna with distinct horizontal and vertical polarizations. As shown in Figure 4c, the fabricated sample realizes beam splitting functionality for LHCP and RHCP output waves at ±30°, respectively, in the folding state ($d = 0$). In the unfolding state ($d = 15$ mm), the main beam (θ_0) appeared at ≈ ±14°, respectively, where their first-order mode

also occurred at $\theta_1 = -47°$ for LHCP and +47° for RHCP waves. From the experimental results in Figure 4c,d, it is important to conclude that the proposed metasurface can simultaneously realize beam splitting and steering between LHCP and RHCP waves. All the results show their good agreement between theoretical prediction, numerical simulation, and measurement. Minor deviations in the results were due to fabrication tolerances and unexpected errors in manual measurement. It should be noted that there must be electromagnetic wave leakage when the spatial distance between the metastrips is presented (Figure S2, Supporting Information). However, the reflected power of the main beams between folded and unfolded states is still comparable, as shown in Figure S3, Supporting Information. Thus, the proposed concept design was successfully fabricated and demonstrated.

3. Conclusion

In this study, we have proposed a spatial modulation metasurface which could achieve beam splitting and steering for circular polarized electromagnetic wave. The beam splitting functionality between LHCP and RHCP is obtained by designing the nonuniform phase distribution on the metasurface following the geometric phase concept. On the other hand, the beam steering capability for both LHCP and RHCP output waves is realized based on the spatial modulation mechanism between each metastrip. Finally, we fabricated the proposed structure using 4D printing technology to provide additional mechanical deformable and self-recovery characteristics depending upon the heating temperature. The measured results show very good agreement with the theoretical prediction and numerical simulation. The proposed spatial modulating metasurface offers a new design methodology to control electromagnetic waves without relying solely on metasurface element phase distributions. Moreover, the fabricated sample is simpler in structure, cheaper to produce, and can achieve reconfigurable electromagnetic functionality. Therefore, it has the potential to be developed for mechanical or smart materials-based electromagnetic devices.

4. Experimental Section

Numerical Simulations: All numerical simulations were performed using a frequency-domain solver from the commercial software Ansys high-frequency structure simulator (HFSS). Simulated reflection magnitudes and phases for each unit cell were obtained by considering a single unit cell under normal incident plane wave illumination with master/slave setup with periodic boundary conditions. Far-field scattering pattern outcomes were obtained by simulating actual (finite size) structures with perfectly matched layer (PML) boundary. A normally incident plane wave with an electric field along the metastrips was assumed to calculate far-field scattering patterns using the Ansys HFSS simulator.

Sample Fabrication: The proposed mechanical tunable metasurface was fabricated as follows. Eight metastrips were manufactured with HT filament using Sindoh 3DWOX 7X 3D printer with 80% infill density. Then the conductive pattern (Ag-520EI silver conductive ink) was printed on top of the metastrips by screen printing (DY-8120NM Screen Print Press). A copper tap was used as the ground for all eight metastrips. Post-processing was required after screen printing to increase conductive pattern conductivity. The fabricated sample was thermal sintered at 100 °C for 20 min in an SH Scientific SH-VDO-30NS vacuum drying oven. The supporting mechanism was fabricated by printing HT filament and SMP simultaneously (3DWOX 7X 3D printer, Figure S1, Supporting Information). Finally, the eight metastrips were connected to the supporting mechanism using bounding film to produce the final sample, as shown in Figure 4a.

Experimental Measurements: Figure 4b shows the measurements setup for the microwave region. Two X-band horn antennae were used as transmitter (Tx) and receiver (Rx) connected to N9918A FieldFox Handheld Microwave Analyzer ports 1 and 2, respectively. The receiver antenna was used to measure the electric field magnitudes and phases with horizontal and vertical polarizations, and subsequently derive the scattering patterns shown in Figure 4c,d.

Supporting Information

Supporting Information is available from the Wiley Online Library or from the author.

Acknowledgements

This work was supported by the National Research Foundation of Korea (NRF) grant funded by the Korea government (MSIT) (2021R1A2C3005239).

Conflict of Interest

The authors declare no conflict of interest.

Data Availability Statement

Research data are not shared.

Keywords

beam splitting, beam steering, metasurfaces, self-deformation, spatial modulation

Received: April 26, 2021
Revised: May 6, 2021
Published online:

[1] J. B. Pendry, D. Schurig, D. R. Smith, *Science* **2006**, *312*, 1780.
[2] D. R. Smith, W. J. Padilla, D. C. Vier, S. C. Nemat-Nasser, S. Schultz, *Phys. Rev. Lett.* **2000**, *84*, 4184.
[3] J. B. Pendry, A. J. Holden, D. J. Robbins, W. J. Stewart, *IEEE Trans. Microwave Theory Tech.* **1999**, *47*, 2075.
[4] D. R. Smith, J. B. Pendry, M. C. K. Wiltshire, *Science* **2004**, *305*, 788.
[5] N. Kundtz, D. R. Smith, *Nat. Mater.* **2010**, *9*, 129.
[6] M. Khorasaninejad, F. Capasso, *Science* **2017**, *358*, eaam8100.
[7] D. Schurig, J. J. Mock, B. J. Justice, S. A. Cummer, J. B. Pendry, A. F. Starr, D. R. Smith, *Science* **2006**, *314*, 977.
[8] H. Chu, Q. Li, B. Liu, J. Luo, S. Sun, Z. H. Hang, L. Zhou, Y. Lai, *Light Sci. Appl.* **2018**, *7*, 50.

[9] C. Huang, J. Yang, X. Wu, J. Song, M. Pu, C. Wang, X. Luo, *ACS Photonics* **2017**, *5*, 1718.
[10] A. Arbabi, E. Arbabi, Y. Horie, S. M. Kamali, A. Faraon, *Nat. Photonics* **2017**, *11*, 415.
[11] A. Díaz-Rubio, V. S. Asadchy, A. Elsakka, S. A. Tretyakov, *Sci. Adv.* **2017**, *3*, e1602714.
[12] M. Moccia, S. Liu, R. Y. Wu, G. Castaldi, A. Andreone, T. J. Cui, V. Galdi, *Adv. Opt. Mater.* **2017**, *5*, 1700455.
[13] L. Huang, X. Chen, H. Mühlenbernd, H. Zhang, S. Chen, B. Bai, Q. Tan, G. Jin, K.-W. Cheah, C.-W. Qiu, J. Li, T. Zentgraf, S. Zhang, *Nat. Commun.* **2013**, *4*, 2808.
[14] H. Ren, G. Briere, X. Fang, P. Ni, R. Sawant, S. Héron, S. Chenot, S. Vézian, B. Damilano, V. Brändli, S. A. Maier, P. Genevet, *Nat. Commun.* **2019**, *10*, 2986.
[15] A. Silva, F. Monticone, G. Castaldi, V. Galdi, A. Alù, N. Engheta, *Science* **2014**, *343*, 160.
[16] N. Mohammadi Estakhri, B. Edwards, N. Engheta, *Science* **2019**, *363*, 1333.
[17] M. Camacho, B. Edwards, N. Engheta, *Nat. Commun.* **2021**, *12*, 1466.
[18] H. J. Visser, *Array and Phased Array Antenna Basics*, John Wiley & Sons, Inc., Chichester, UK **2006**.
[19] R. Bansal, *Antenna Theory: Analysis and Design*, John Wiley & Sons, Inc., Hoboken, NJ **2005**.
[20] D. M. Pozar, *Microwave Engineering*, John Wiley & Sons, Inc., Hoboken, NJ **2012**.
[21] N. Yu, P. Genevet, M. A. Kats, F. Aieta, J.-P. Tetienne, F. Capasso, Z. Gaburro, *Science* **2011**, *334*, 333.
[22] T. J. Cui, M. Q. Qi, X. Wan, J. Zhao, Q. Cheng, *Light Sci. Appl.* **2014**, *3*, e218.
[23] L. Li, T. Jun Cui, W. Ji, S. Liu, J. Ding, X. Wan, Y. Bo Li, M. Jiang, C.-W. Qiu, S. Zhang, *Nat. Commun.* **2017**, *8*, 197.
[24] J. Y. Dai, J. Zhao, Q. Cheng, T. J. Cui, *Light Sci. Appl.* **2018**, *7*, 90.
[25] H. Wu, S. Liu, X. Wan, L. Zhang, D. Wang, L. Li, T. J. Cui, *Adv. Sci.* **2017**, *4*, 1700098.
[26] B. Y. S. Pancharatnam, *Proc. Ind. Acad. Sci. USA* **1956**, *44*, 247.
[27] M. V. Berry, *J. Mod. Opt.* **1987**, *34*, 1401.
[28] L. Zhang, S. Liu, L. Li, T. J. Cui, *ACS Appl. Mater. Interfaces* **2017**, *9*, 36447.
[29] R. C. Devlin, A. Ambrosio, N. A. Rubin, J. P. B. Mueller, F. Capasso, *Science* **2017**, *358*, 896.
[30] J. P. Balthasar Mueller, N. A. Rubin, R. C. Devlin, B. Groever, F. Capasso, *Phys. Rev. Lett.* **2017**, *118*, 113901.
[31] M. R. Akram, G. Ding, K. Chen, Y. Feng, W. Zhu, *Adv. Mater.* **2020**, *32*, 1907308.
[32] Y. Yuan, S. Sun, Y. Chen, K. Zhang, X. Ding, B. Ratni, Q. Wu, S. N. Burokur, C. W. Qiu, *Adv. Sci.* **2020**, *7*, 2001437.
[33] Y. Yuan, K. Zhang, B. Ratni, Q. Song, X. Ding, Q. Wu, S. N. Burokur, P. Genevet, *Nat. Commun.* **2020**, *11*, 4186.
[34] S. C. Malek, H. S. Ee, R. Agarwal, *Nano Lett.* **2017**, *17*, 3641.
[35] C. Zhang, J. Jing, Y. Wu, Y. Fan, W. Yang, S. Wang, Q. Song, S. Xiao, *ACS Nano* **2020**, *14*, 1418.